Research Article

Study on Mechanical Properties and Energy Consumption of Fissured Sandstone with Different Dip Angles under Impact Load

Qi Ping [ID],[1,2,3] **Shuo Wang,**[2,3] **Yulin Wu,**[2,3] **Shijia Sun,**[2,3] **Kaifan Shen,**[2,3] **Chen Wang,**[2,3] **Qi Gao,**[2,3] **and Chenglong Fang**[2,3]

[1]*State Key Laboratory of Mining Response and Disaster Prevention and Control in Deep Coal Mine, Anhui University of Science and Technology, Huainan, Anhui 232001, China*
[2]*Research Center of Mine Underground Engineering, Ministry of Education, Anhui University of Science and Technology, Huainan, Anhui 232001, China*
[3]*School of Civil Engineering and Architecture, Anhui University of Science and Technology, Huainan, Anhui 232001, China*

Correspondence should be addressed to Qi Ping; ahpingqi@163.com

To study the dynamic mechanical properties and energy consumption of fissured sandstone with different dip angles under impact load, impact compression tests were conducted on seven groups of and intact and fractured sandstone specimens with different dip angles using the split Hopkinson pressure bar (SHPB) device with 0.3 MPa air pressure. The influence of dip fissures on the crushing shape, dynamic compressive strength, dynamic elastic modulus, dynamic peak strain, dynamic average strain rate, dynamic stress-strain curve, and energy consumption of rock specimens was systematically analyzed. The results show that the 45° fissure angle is the best fragile angle according to the failure mode and dynamic compressive strength of the specimen and that difference in specimen failure modes specimens is attributed to the existence of fractures with different dip angles. The dynamic elastic modulus reaches the minimum when the fissure angle is 45° and the maximum when the fissure angle is 90°. The dynamic peak strain is the lowest and minimal influence of fissure angle on the average strain rate of the specimen is presented when the fissure angle is 45°. From the stress-strain curves, the two specimen ends are most vulnerable to the relative sliding and dislocation of the lateral fissure angle during impact compression when the fissure angle is 45°. With stable incident energy in the test, a prominent relationship exists between the reflected energy, transmission energy, and energy consumption and the fissure angles. In addition, the fissure angle exhibits a prominent influence on reflected energy and the energy consumption of the specimen when the fissure angle ranges from 45° to 60°.

1. Introduction

In nature, rocks contain a large number of fissures due to long-term geological movement. These fissures are widely distributed and form complex joint structures, which have certain regularity. They extend to all rock strata and cause many problems in practical engineering. For example, in water conservancy and hydropower projects, rock foundation excavation of hydraulic structures [1, 2] would be accelerated if the problem of rock fissures is understood correctly. During blasting of mining resources [3], rock discontinuity can hinder the propagation of stress waves, which leads to serious energy consumption, and budget cost.

Subway, as an indispensable part of urban development, usually encounters hard rock obstacles in shield construction [4, 5]. By studying the rock crack inclination, the broken easy direction of the rock can be quickly judged. With the proposal of the national "14th Five Year Plan" strategy, the state plans to speeds up the construction of new infrastructure. Therefore, it is urgent to study the problem of fissured rock mass.

Scholars have carried out numerous research work on rock fissures and achieved remarkable results. Tang et al. [6] used the modified split Hopkinson pressure bar (SHPB) to realize the combined dynamic and static loading of rocks, and then studied the mechanical properties of skarn under

the combined action of one-dimensional static load and cyclic impact. Han et al. [7] studied the influence of surface roughness on the shear behaviors of rock joints under constant normal load and stiffness boundary conditions. Zhong et al. [8] investigated the effect of in situ leaching solution of ion-absorbed rare earth on the mechanical behavior of basement rock. Luo et al. [9] revealed the linear energy storage and dissipation laws of intact rock under three-point bending, and discussed the influence of preexisting defects on the linear energy storage and dissipation laws. Cheng et al. [10, 11] explored the mechanical properties of salt rock under thermal-hydro-mechanical (THM) coupling conditions through an extremely long-term creep test, and proposed a nonlinear creep-damage constitutive model. Kulatilake et al. [12] studied the relationship between mechanical parameters of jointed rock mass and rock mass structure using the prefabricated joints and similar material model test. Through study of acoustic emission and crack propagation characteristics of variable angle jointed sandstone, Chen et al. [13] found that when the joint angle was 60°, serious fracture phenomenon occurred and the energy released during crack formation was the largest. He et al. [14] conducted the cyclic loading test on sandstone under different stress amplitudes and studied the deformation characteristics, cyclic softening, cyclic hardening, and energy consumption characteristics during the three deformation stages in the cyclic loading process. Li et al. [15] modified the split Hopkinson pressure bar which can realize the coupling effect of axial static prestress, axial impact load, and optional confining pressure of rock specimens. Li et al. [16] investigated the static-dynamic coupling loading mechanical characteristics and failure law of fractured granite using an improved SHPB device. Wang et al. [17] used the split Hopkinson pressure bar (SHPB) device to perform simulation impact test of jointed rocks with different inclination angles with mortar. They obtained the influence of joint dip angle on impact energy transmission of rock-like materials and presented the expression of energy loss ratio with joints. Wang et al. [18] conducted the triaxial compression test and acoustic test on sandstone with different joint dip angles under different confining pressures. They reported that the joint dip angle of 60° had a great impact on the strength and physical characteristics of sandstone. Ma et al. [19] discussed the dynamic failure characteristics of sandstone in the deep roadways with different joint dip angles in terms of SHPB tests. These results demonstrate that with increasing joint dip angle, the dynamic compressive strength and peak strain of sandstone first decrease and then increase, and the plasticity decreases brittleness increases monotonically. The final failure mode of sandstone can be divided into splitting tensile failure, mixed shear-tensile composite failure, and shear failure. Deng et al. [20] studied the influence of joint dip angle on the deformation and strength characteristics and failure mode of intermittent jointed rock mass. Pan et al. [21] prefabricated cement mortar specimens with different joint dip angles and conducted an impact test with a SHPB device. They found that the specimen is more likely to be damaged when joint angles are 45° to 60°. When the action direction of external loads is 30° to 45° with the joint, the specimen is most conducive to crushing.

To study the energy dissipation characteristics of sandstone specimens under impact load, Ping et al. [22] used three air pressures to conduct SHPB compression tests with different impact rates. They concluded that the ratio of absorbed energy to incident energy was constant, and the crushing energy consumption density was linearly related to the incident energy. The greater the crushing energy consumption density, the more broken the specimen was. The energy absorbed was mainly dissipated for the damage evolution and deformation of the rock, so the crushing energy dissipation density was used to reflect the strength characteristics of sandstone under impact loads. Li et al. [23] conducted a one-dimensional coupled dynamic and static loading test with medium and high strain rates through the modified SHPB device. The results indicated that the coupled dynamic and static strength of siltstone was greater than that under pure static or simple dynamic load, and the strength of siltstone increased with strain rate. Hu et al. [24] found that an increase in roughness, the contact area of water-rock interaction was improved, and the weakening degree of water on the shear strength of the joint surface also increased. Zhang et al. [25] studied the constitutive model of rock mass with initial joint damage. They observed that when the joint dip angles were 0° and 90°, the initial damage and critical damage of rock mass were small, and the peak strength was large. When the joint dip angle was 60°, the initial damage and critical damage of rock mass were large, and the peak strength was small. Li et al. [26] demonstrated that the strain rate and dynamic elastic modulus of the specimen increased, and the specimen was fractured slightly. With the increase of joint dip angle, the peak strength was lower, and the jointed specimen presented a greater change of energy dissipation rate versus the strain rate than the intact specimen. Li et al. [27] studied the relationship between postpeak stress-strain curve, failure mode, postpeak residual strength, postpeak Poisson ratio, and joint dip angle of rock-like specimens under uniaxial compression. Yang et al. [28] used filling material to simulate the jointed rock and gave its dynamic elastic modulus. The dynamic compressive strength decayed exponentially with decreasing strength of the filling material. Meantime, the reflected energy ratio increased with a decrease in strength of the filling material. The energy dissipation of the specimen was related to the properties of the filling material. Ju et al. [29] performed the SHPB compression test on artificial jointed specimens with varied roughness to study the relationship between energy dissipation and fractal dimension.

At present, most research on the angular properties of rock fractures is based on static tests. Although a small number of dynamic tests are carried out using SHPB, they use rock-like materials such as cement mortar and gypsum to simulate fractured rocks with different dip angles. There are few reports on rock fractures in dynamic tests. Therefore, in this paper, the dynamic characteristics of single fissured rock mass were studied, because the prefabricated single fissured rock mass was fundamental for the study of multi fractured rock mass. The sandstone from Dingji mine in

Huainan City, Anhui Province was selected to prepare seven dip angles through fissures along the full-face of specimens. Firstly, basic physical quantities of sandstone specimens with fissure angles of 0°, 15°, 30°, 45°, 60°, 75°, and 90° were measured. Then the dynamic compression test was carried out on each group of specimens using 0.3 MPa air pressure to observe the crushing morphology of fissured sandstone. Finally, the dynamic compressive strength, dynamic elastic modulus, dynamic peak strain, dynamic average strain rate, dynamic stress-strain curve, and the relationship between energy consumption and fissure angle were analysed. This paper provides theoretical guidance for rock engineering design and economical construction.

2. Specimen Preparation and Test Process

2.1. Specimen Preparation. The sandstone used in this test is from the Dingji Coal Mine of Huainan Mining Group. In order to ensure the accuracy of test results, the sandstone samples were prepared from the same rock block. The specimen size is Φ 50 mm × 50 mm, and specimens were prepared in strict accordance with the procedures of International Society for Rock Mechanics (ISRM) [30] and those for rock dynamic characteristics of Chinese Society of Rock Mechanics and Engineering [31]. The diameter error of specimens is ≤0.3 mm, the inequality of the two ends is ≤0.05 mm, and the maximum angle error between the two ends and the central axis is ≤0.25°.

Rock blocks were cored, cut, and polished to obtain specimens with required sizes. Then, seven inclination angles were made through a numerical control stone mechanism according to fissures along the full-face of the specimen (Figure 1). The inclination angles are 0°, 15°, 30°, 45°, 60°, 75°, and 90°, respectively. The fissure length and width are 2 cm and 2 mm, respectively, and the fissure is always required to be evenly divided by the central axis of the specimen. Four specimens were required each fissure angle groups, and plus 4 specimens for the intact group, with a total of 32 specimens. The prepared specimens are shown in Figure 2.

2.2. Test Scheme

(1) To ensure the accuracy of test data, the basic physical parameters of each specimen were first measured, and rock specimens with large differences were excluded.

(2) The specimen was placed on the SHPB device. The dynamic compression test was carried out with 0.3 MPa air pressure, and the waveform was collected by strain gauge. Attained data were processed to analyze the dynamic mechanical properties of sandstone with different fissure angles.

2.3. SHPB Test System. As shown in Figure 3, the dynamic compression test was conducted on the SHPB device of the State Key Laboratory of mining response and disaster prevention and control of deep coal mine.

Aiming at the occurrence state of high ground stress and high impact disturbance during deep rock mining, the SHPB
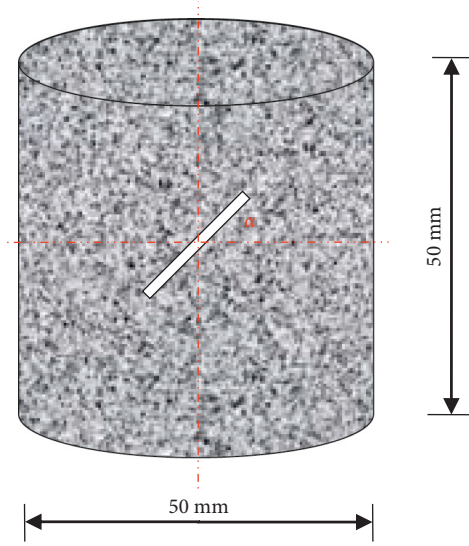

FIGURE 1: Size of a fissured rock specimen.

system can be used to study the dynamic compression, tension, and shear characteristics, and the failure mode of multifield and multiphase coupling rock mass, so as to obtain rock parameters including the impact dynamic strength, energy consumption, impact loading waveform, strain rate effect, and stress wave propagation characteristics. The incident bar, transmitted bar, absorbing bar, and impact bullet of the SHPB system have a yield strength greater than 800 MPa and a diameter of 50 mm. Medium strain rate ($101{\sim}103s^{-1}$) can be achieved by the SHPB system. In this experiment, the fusiform bullet was used, and nitrogen was used as the impact pressure. The bullet was required to be pushed to the same position of launch chamber each time to ensure the comparability of test results. During the impact compression test, a rock specimen was coaxially clamped between the incident and transmitted bars. With the incident wave passing through the specimen, the data acquisition system can record the voltage-time curve. By measuring the voltage of strain gauges on the incident and transmitted bars, dynamic mechanical parameters such as stress, strain, and strain rate stress of the specimen can be indirectly calculated.

According to the basic principle of SHPB test [32], three dynamic mechanical parameters, i.e., the stress $\sigma(t)$, strain $\varepsilon(t)$, and strain rate $\dot{\varepsilon}(t)$, can be calculated through the following equation:

$$\left.\begin{aligned} \sigma(t) &= \frac{E_0 A_0}{2A_s}\left[\varepsilon_I(t) + \varepsilon_R(t) + \varepsilon_T(t)\right] \\[2mm] \varepsilon(t) &= -\frac{C_0}{L_s}\int_0^r \left[\varepsilon_I(t) + \varepsilon_R(t) - \varepsilon_T(t)\right]dt \\[2mm] \varepsilon(t) &= -\frac{C_0}{L_s}\left[\varepsilon(t) + \varepsilon(t) - \varepsilon_T(t)\right] \end{aligned}\right\}, \quad (1)$$

where $A0$ and AS represent the cross-sectional area of the SHPB bars and rock specimens, respectively; $E0$ and $C0$ are the elastic modulus and longitudinal wave velocity of the
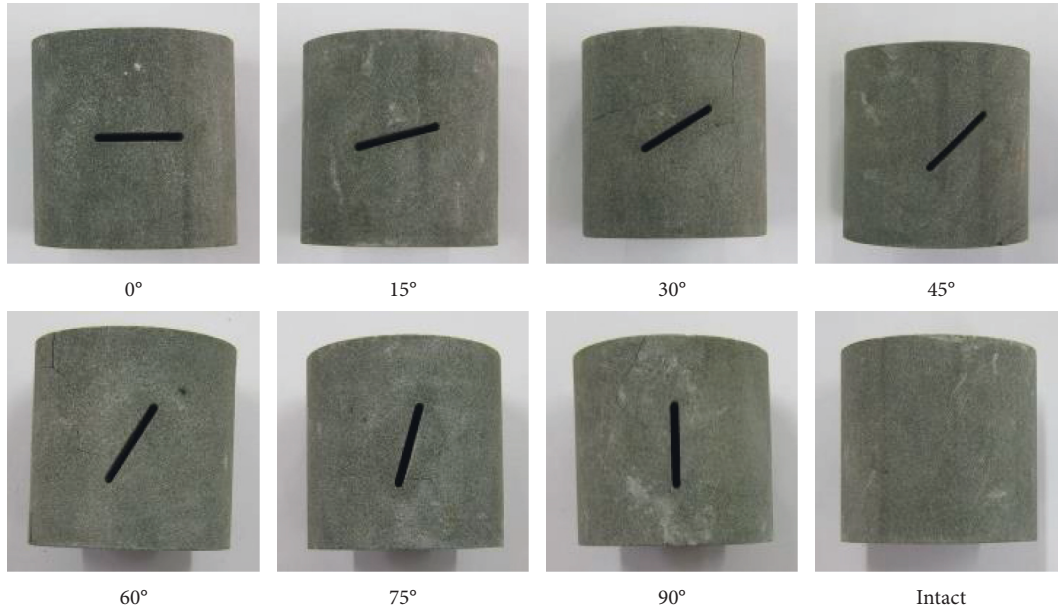
Figure 2: Prepared specimens.

Figure 3: Split Hopkinson pressure bar test system.

SHPB bars, respectively; LS is the specimen length; $\varepsilon I(t)$, $\varepsilon R(t)$, and $\varepsilon T(t)$ are the incident, reflected, and transmitted stress wave at time t; Positive direction of compressive stress; and T is the propagation duration of stress waves.

3. Experimental Results and Analysis

3.1. Determination of Basic Physical Quantity of Rock Specimens. The mass, diameter, height of 32 rock specimens, as well as the angle, length, and width of contained fissures were measured by electronic scale and vernier caliper as shown in Table 1.

3.2. Failure Mode of Specimens. The failure modes of sandstone specimens with seven fissure angles and the intact specimen are shown in Figure 4.

From the specimen failure modes, it was found that with the fissure angle increasing from 0° to 45°, the specimen fragments gradually increase, and the dynamic compressive strength decreases gradually according to the preliminary judgment. When the fissure angles varied from 60° to 90°, cracks expanded from the fissure dip angle to the sides, producing few fragments with a good shape. It is

Table 1: Basic physical parameters of rock specimens.

Fissure dip angle	Test piece number	Mass (g)	Diameter (mm)	Height (mm)
0°	DJ16-01	237.64	50.26	48.95
	DJ16-02	241.67	49.99	49.75
	DJ16-03	245.21	50.29	50.26
	DJ16-04	243.94	50.08	50.10
15°	DJ16-05	240.35	50.21	49.61
	DJ16-06	243.28	50.14	49.92
	DJ16-07	242.81	50.02	49.72
	DJ16-08	241.57	49.85	49.69
30°	DJ16-09	243.06	50.09	50.11
	DJ16-10	242.53	50.11	49.93
	DJ16-11	243.33	49.98	49.98
	DJ16-12	244.52	50.18	50.33
45°	DJ16-13	243.04	50.10	49.82
	DJ16-14	240.91	50.05	49.33
	DJ16-15	243.56	50.11	50.19
	DJ16-16	239.39	49.91	49.67
60°	DJ16-17	245.31	50.09	50.27
	DJ16-18	244.61	50.19	50.03
	DJ16-19	242.72	50.23	49.83
	DJ16-20	240.51	50.28	49.66
75°	DJ16-21	245.50	50.18	50.13
	DJ16-22	246.15	50.16	50.22
	DJ16-23	243.31	50.17	50.20
	DJ16-24	245.92	50.22	50.32
90°	DJ16-25	246.47	50.13	50.42
	DJ16-26	240.16	50.15	49.53
	DJ16-27	238.34	50.36	49.31
	DJ16-28	243.66	50.09	50.29
Intact	DJ16-29	250.78	49.97	50.43
	DJ16-30	250.27	49.99	50.34
	DJ16-31	249.84	49.97	50.25
	DJ16-32	247.91	49.98	50.05

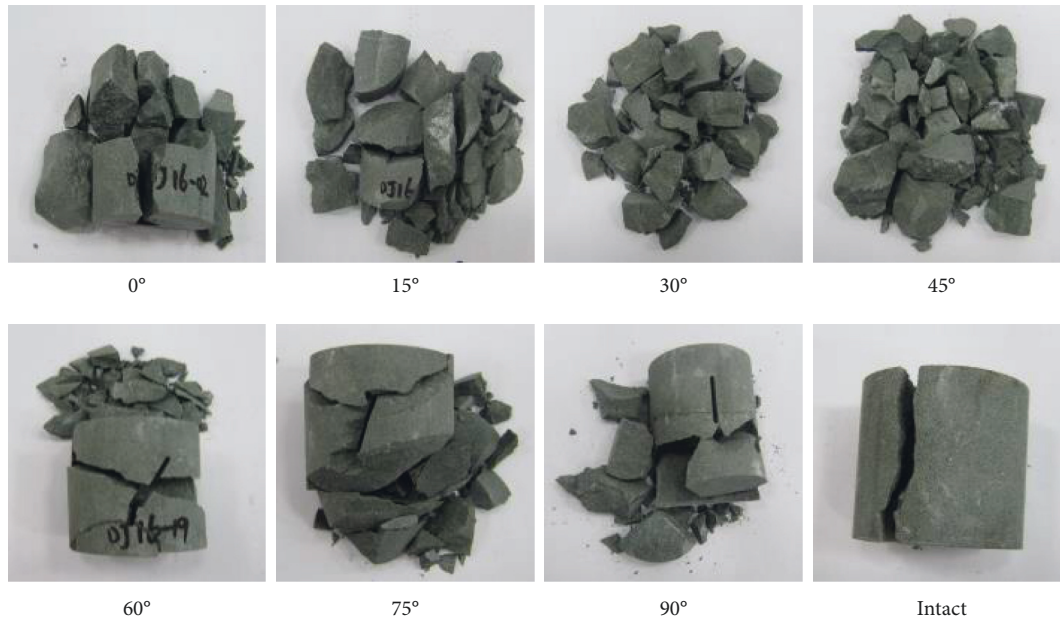| 0° | 15° | 30° | 45° |
| 60° | 75° | 90° | Intact |

FIGURE 4: Specimen destruction morphology.

preliminarily judged that the dynamic compressive strength increases gradually. When intact specimen was impacted by the incident bar, the two ends were cracked along the axial direction of the specimen, and no cracks or fragments appeared in other places. Thus, the specimen is the most vulnerable to damage and the best fragile when the fissure angle is 45°.

The existence of fissure angle is the main reason for difference in failure modes of specimens, which causes local stress concentration and leads to uneven stress in the entire specimen. When the specimen end faces were subjected to external force, sliding dislocation appeared at the inclined fissure, and produced a shear stress along the inclined crack surface. It reduced the specimen strength and caused breakage. This phenomenon can be observed from the failure modes of specimens with fissure angles of 60°, 75°, and 90°.

3.3. Dynamic Compressive Strength.

The dynamic compressive strength and related average value of specimens with different fissure angles are shown in Figure 5.

It can be seen from Figure 5 that under 0.3 MPa air pressure, fissures with different dip angles have an obvious influence on the dynamic compressive strength of sandstone specimens. The intact sandstone specimen displays the greatest dynamic compressive strength with an average of 56.39 MPa. With increasing fissure angle from 0° to 45°, the average dynamic compressive strength decreases monotonically. The dynamic compressive strengths are 29.51, 24.77, 23.71, and 21.11 MPa, with reductions accounting for 52.3%, 44.0%, 42.0%, and 37.4%, respectively. As fissure angle increase from 60° to 90°, the average value of dynamic compressive strength increase from 28.32 to 30.85, and then to 33.20 MPa, with increments accounting for 50.2%, 54.7%, and 58.9% of average dynamic compressive strength of intact
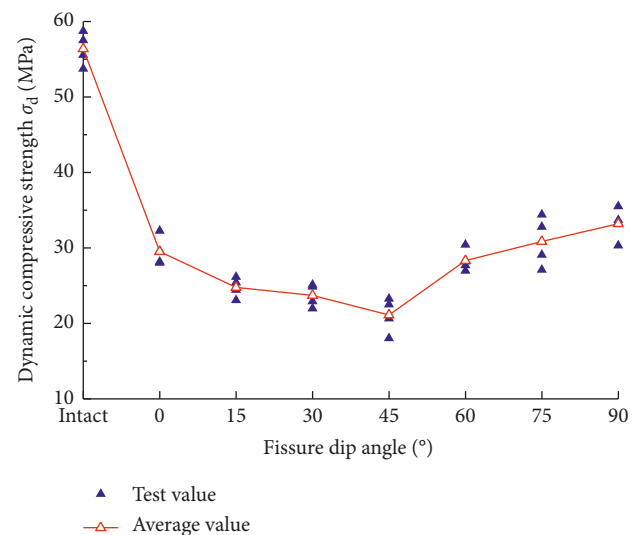

FIGURE 5: Relationship between the fissure angle and dynamic compressive strength.

specimens, respectively. Therefore, it is concluded that the average dynamic compressive strength reaches the minimum when the fissure angle is 45° which can be called the most favorable crushing angle. The above analysis is basically consistent with the specimen failure modes in Figure 4.

3.4. Dynamic Elastic Modulus.

The variations in dynamic elastic modulus E_d of specimens with different fissure angles are shown in Figure 6.

It can be seen from Figure 6 that the dynamic elastic modulus first decreases and then increases as the fissure angle increases, and that it reaches the minimum at 45° fissure angle. These results reveal that the fissure angle of 45° has the most significant effect on the dynamic elastic modulus.

FIGURE 6: Relationship between the fissure angle and dynamic elastic modulus.
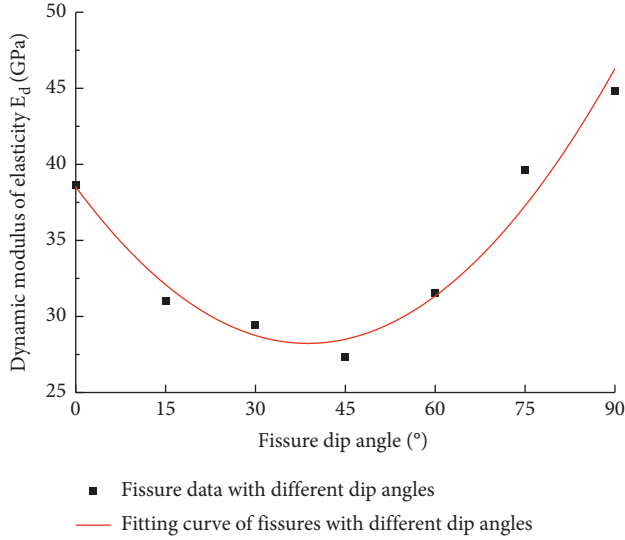

FIGURE 7: Relationship between the fissure angle and dynamic peak strain.

By fitting method, the fissure angle was found to have a quadratic function relationship with the dynamic elastic modulus, with a correlation of determination R2 of 0.9734, as shown in the following equation:

$$E_d = -6.87 \times 10^{-3}\alpha^2 - 0.532\alpha + 38.519 \left(R^2 = 0.9734\right), \quad (2)$$

where E_d is dynamic elastic modulus and α is the fissure angle.

3.5. Dynamic Peak Strain and Average Strain Rate.

The dynamic peak strain ε_d of specimens with different fissure angles is shown in Figure 7.

It can be seen from Figure 7 that the fissure angle is related to the dynamic peak strain in a quadratic relation ($R2 = 0.9587$), as expressed by the following equation:

$$E_d = 2.30 \times 10^{-4}\alpha^2 - 0.019\alpha + 3.38 \left(R^2 = 0.9587\right). \quad (3)$$

The dynamic peak strain of sandstone specimens decreases rapidly with the increase of fissure angle from 0° to 15°, decreases slowly when the fissure angel varies from 15° to 45°, and subsequently reaches the minimum at 45° fissure angle. After that, it starts to rise gradually at 45° to 75° fissure angle, and the rising trend from 75° to 90° fissure angle is accelerated, finally reaching the maximum at 90° fissure angle. These results demonstrate that fissures with different dip angles have a prominent impact on the dynamic peak strain. When the fissure angle is 45°, the dynamic peak strain is the minimum.

The dynamic average strain rate ε_c of fissured specimens with different dip angles is shown in Figure 8.

It can be seen from Figure 8 that fissure angle has a quadratic function relationship with the average strain rate, and that the correlation $R2$ coefficient reaches 0.9727, as described by the following equation:
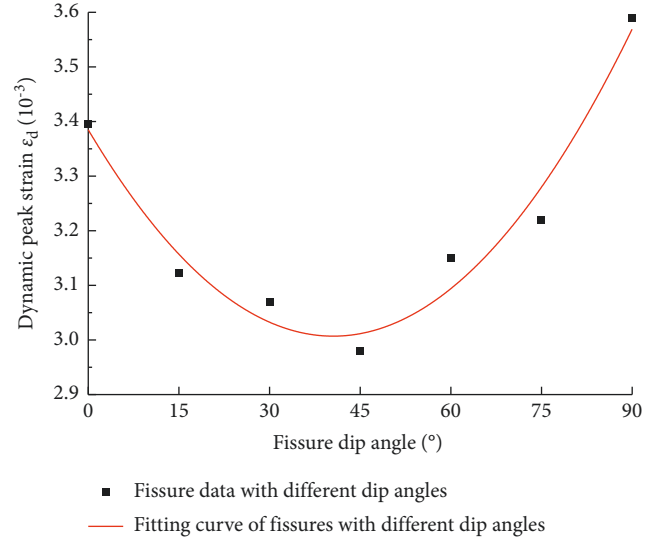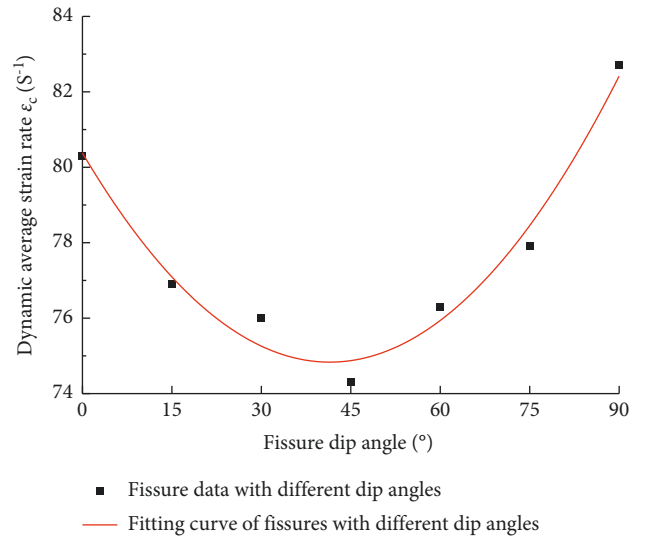

FIGURE 8: Relationship between the fissure angle and dynamic average strain rate.

$$\varepsilon_c = 3.22 \times 10^{-3}\alpha^2 - 0.260\alpha + 80.271 \left(R^2 = 0.9727\right). \quad (4)$$

With increasing fissure angle from 0° to 45°, the average strain rate of sandstone specimens decreases rapidly and reaches the minimum at 45°. Subsequently, it rise speedily when fissure angle changes from 45° to 90° and reaches the maximum at 90°. It can be concluded that when the fissure angle is 45°, the influence of a single fissure on the average strain rate of sandstone specimens is the smallest.

3.6. Dynamic Stress-Strain Curve.

Dynamic compression tests were carried out on 7 groups of fissured specimens with different dip angles and intact specimens. Representative
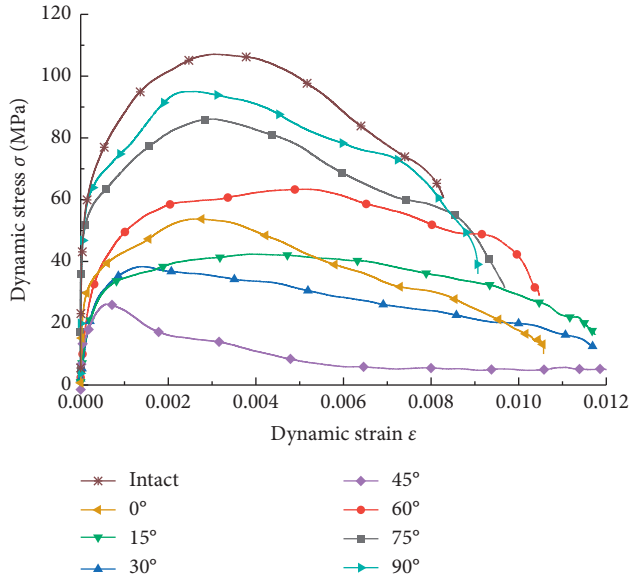
FIGURE 9: Representative dynamic stress-strain curves of specimens with different fissure angles.

data were selected to draw the dynamic stress-strain curve, as shown in Figure 9.

It can be seen from Figure 9 that the sandstone specimen has an elastic deformation stage at the initial impact compression. At this time, the curve rises approximately a straight line and then upward convex. As indicated by the approximate straight line, the intact specimen presents the largest elastic modulus and the fissured specimen with an dip angle of 45° yields the smallest elastic modulus. In the convex state, an elastic gradual unloading phenomenon caused by the relative slip and dislocation at the dip fissure occurs, and this phenomenon is the most obvious 45° fissure angle. After the elastic deformation stage to the peak stress, and the elastic unloading occurs at the highest point. It can be seen that the intact specimen displays the greatest peak stress, and the peak stress of the specimen with 45° fissure angle is the smallest. Then, dip crack of each specimen group begins to expand around the side and results in an extremely uneven stress inside the specimen, and thus leading to the plastic specimen deformations. In the plastic stage, the curve slope indicates that plastic deformation occurs most slowly in intact specimen and fissured specimens with dip angles of 90° and 75°, while the plastic deformation occurs gradually when fissure angles are 15°, 30°, and 45°. Among them, the plastic deformation in specimens with 45° fissure angle is the fastest with an increase in stress. When the specimen with 45° fissure angle is subjected to impact compression, both ends of the specimen are most vulnerable to fracture due to the relative sliding and dislocation of fracture surface dip angle.

3.7. Energy Consumption of Specimens. During the SHPB test, the energy consumption of rock is irreversible. Ignoring the energy loss of contact surfaces between the incident and transmitted bars and the rock specimen, the incident wave energy *EI*, reflected wave energy *ER*, transmitted wave energy *ET* and loss energy *ED* of the rock specimen has the following relation [33]:

$$E_I = E_R + E_T + E_D, \tag{5}$$

where *EI*, *ER*, and *ET* are the incident wave energy, reflected wave energy, and transmitted wave energy, respectively. The three energies can be calculated by the following equation:

$$\left. \begin{aligned} E_I &= A_0 C_0 E_0 \int_0^t \varepsilon_I^2(t)dt \\ E_R &= A_0 C_0 E_0 \int_0^t \varepsilon_R^2(t)dt \\ E_T &= A_0 C_0 E_0 \int_0^t \varepsilon_T^2(t)dt \end{aligned} \right\}. \tag{6}$$

The incident wave energy *ET*, reflected wave energy *ER*, transmitted wave energy *ET* and loss energy *ED* of each group of specimens are obtained and listed in Table 2.

Although 0.3 MPa air pressure was used in each group during the impact test, in order to reduce the incident energy and analyze the difference in the test results, the energy proportion method was adopted. That is, the *ER/EI*, *ET/EI*, and *ED/EI*, were adopted to describe the energy proportion of specimens with different fissure angles, as shown in Figure 10.

Figure 10 shows the changes in ER/EI with the fissure angle: The ER/EI increases gradually from intact sandstone to 45° fissured specimen, in which the increase rate of ER/EI from intact sandstone to 0° fissured specimen is greater than that from 0° to 45° fissured angle. However, the ER/EI of specimens with fissure angle from 45° to 60° decreases gradually. The ER/EI increases slightly when the fissure angle varies from 60° to 90°. The proportion of reflected energy of sandstone specimens with fissure angles of 45° to 60° becomes a turning interval in the process of the intact specimen to the 90° fissured specimen.

In the test, the ET/EI changes with the fissure angle. It decreases gradually from intact sandstone to the 30° fissured specimen, in which the decline rate of ET/EI is greater from intact sandstone to 0° fissured specimen relative to specimens with fissure angle from 0° to 30°. At this time, the 30° fissure angle becomes an inflection point, and the ET/EI of specimens with 30° to 45° fissure angle begin to rise. The ET/EI increases slowly as fissure angle changes from 45° to 90°.

In the test, the ED/EI of the specimen changes with the fissure angle. The ED/EI gradually decreases from the intact specimen to the specimen with 45° fissure angle, and then it remains basically unchanged as the fissure angle changes from 45° to 60°. It increases gradually as the fissure angle varies from 60° to 75°, and finally tends to be stable in the fissure angle range of 75° to 90°. The specimens with fissure angles of 45° to 60° produce the lowest proportion of energy consumption. If the relationship between the incident energy and the specimen energy consumption is fully handled, it can be conducive to rock fragmentation.

To sum up, by ensuring the stability of incident energy in the test, there is a significant relationship between the reflected energy, transmission energy, and energy

TABLE 2: Energy calculations of specimens with different fissure angle in each group.

| Fissure dip angle	Test piece	Energy (J)			
		EI	*ER*	*ET*	*ED*
0°	DJ16-01	58.39	44.21	4.09	10.08
	DJ16-02	56.78	40.74	6.71	9.34
	DJ16-03	55.57	44.54	2.37	8.66
	DJ16-04	58.35	44.04	6.26	8.05
15°	DJ16-05	52.95	43.53	3.43	6.00
	DJ16-06	53.08	40.47	4.90	7.71
	DJ16-07	59.55	48.80	2.06	8.69
	DJ16-08	49.94	38.27	4.57	7.10
30°	DJ16-09	56.52	50.66	1.43	4.42
	DJ16-10	53.58	43.51	2.93	7.14
	DJ16-11	53.87	43.84	2.35	7.68
	DJ16-12	52.80	45.69	1.78	5.33
45°	DJ16-13	52.71	44.62	2.34	5.75
	DJ16-14	53.54	48.19	1.52	3.83
	DJ16-15	58.22	51.15	1.20	5.87
	DJ16-16	57.83	51.84	1.28	4.71
60°	DJ16-17	58.29	48.47	4.49	5.34
	DJ16-18	54.32	45.41	2.87	6.04
	DJ16-19	53.62	44.17	3.59	5.87
	DJ16-20	55.04	51.50	0.24	3.29
75°	DJ16-21	53.99	45.43	3.40	5.16
	DJ16-22	56.44	41.22	7.73	7.49
	DJ16-23	54.09	51.80	0.29	2.01
	DJ16-24	53.78	40.41	6.21	7.16
90°	DJ16-25	49.20	39.04	2.74	7.41
	DJ16-26	63.22	48.60	4.77	9.86
	DJ16-27	55.54	46.82	3.45	5.18
	DJ16-28	57.55	48.75	3.32	5.49
Intact	DJ16-29	51.93	35.75	7.79	8.39
	DJ16-30	51.57	31.08	10.76	9.73
	DJ16-31	56.06	27.74	13.89	14.43
	DJ16-32	48.96	35.22	6.10	7.63
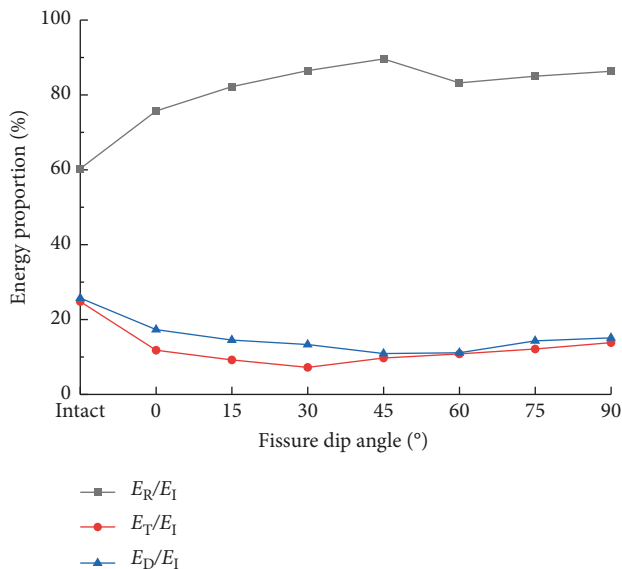
FIGURE 10: Relationship between the energy proportion and fissure angle.

consumption and the fissure angle, and the influence of reflected energy and energy consumption is prominent as the fissure angle ranges from 45° to 60°.

4. Conclusions

(1) When the fissure angle changes from 0° to 90°, the dynamic compressive strength of sandstone specimens first decreases and then increases. It is concluded that the 45° fissure presents the best fragile angle, and the existence of the fissure angle is the main cause for different specimen failure modes.

(2) A quadratic function relationship exists between the fissure angle and the dynamic elastic modulus, and the dynamic elastic modulus reaches the minimum at 45° and the maximum at 90°. Fissures with different dip angles have a prominent influence on the dynamic peak strain and average strain rate of sandstone specimens. The 45° fissure angle produces the minimum dynamic peak strain, and brings the smallest influence on the average strain rate.

(3) During the elastic stage and plastic stage, when the fissure angle of the sandstone specimen is 45°, the two specimen ends are most vulnerable to the relative sliding and dislocation of the fracture on the dip plane when impact compression occurs.

(4) The proportion of reflection energy of sandstone specimens with fissure angle of 45° to 60° is a turning interval from the intact specimen to that with 90° fissure angle. The proportion of transmission energy of sandstone specimen with fissure angle of 30° becomes an inflection point from the intact specimen to that with 90° fissure angle. In addition, the sandstone specimens with fissure angles of 45° to 60° possess the lowest proportion of energy consumption.

Data Availability

The data used to support the findings of this study are available from the corresponding author upon request.

Conflicts of Interest

The authors declare that there are no conflicts of interest regarding the publication of this paper.

Acknowledgments

References

[1] W. Y. Xu, W. T. Zheng, and A. C. Shi, "Classification and quality evaluation of columnar jointed rock mass in hydraulic engineering," *Journal of water conservancy*, vol. 42, no. 3, pp. 262–270, 2011.

[2] Q. Ping, M. J. Wu, and P. Yuan, "Experimental study on dynamic mechanical properties of high temperature sandstone under impact loads," *Chinese Journal of Rock Mechanics and Engineering*, vol. 38, no. 4, pp. 782–792, 2021.

[3] L. Yuan and P. S. Zhang, "Reconstruction and thinking of transparent geological conditions for accurate coal mining," *Journal of coal*, vol. 45, no. 7, pp. 2346–2356, 2020.

[4] Q. Ping, C. L. Zhang, and H. J. Sun, "Experimental study on dynamic characteristics of sandstone after different high temperature cyclings," *Journal of Mining and Safety Engineering*, vol. 38, no. 5, pp. 1015–1024, 2021.

[5] B. Zhu, J. Wang, and Z. Xu, "Mechanical mechanism of construction of new shield tunnel under existing structures," *Journal of Shandong University*, vol. 52, no. 2, pp. 1–8, 2012.

[6] L. Z. Tang, C. Wang, and L. P. Cheng, "Experimental study on the mechanical properties of sika rock under the combined action of one-dimensional static load and cyclic impact," *Journal of Central South University*, vol. 46, no. 10, pp. 3898–3906, 2015.

[7] G. S. Han, Y. Zhou, R. C. Liu, and Q. Tang, "Influence of Surface Roughness on Shear Behaviors of Rock Joints under Constant normal Load and Stiffness Boundary Conditions," *Natural Hazards*, vol. 15, 2022.

[8] W. Zhong, J. Ouyang, D. X. Yang, X. Wang, Z. Guo, and K. Hu, "Effect of the in situ leaching solution of ion-absorbed rare earth on the mechanical behavior of basement rock," *Journal of Rock Mechanics and Geotechnical Engineering*, 2022.

[9] S. Luo and F. Q. Gong, "Linear energy storage and dissipation laws during rock fracture under three-point flexural loading Engineering Fracture Mechanics," vol. 234, no. 7, 2020.

[10] L. Y. Cheng, J. F. Liu, Y. Ren, C. Liang, and Y. Liao, "Study on very long-term creep tests and nonlinear creep-damage constitutive model of salt rock," *International Journal of Rock Mechanics and Mining Sciences*, vol. 146, no. 5, 2021.

[11] L. Y. Cheng, J. F. Liu, Y. Ren, C. Liang, and Y. Zeng, "Mechanical characteristics and permeability evolution of salt rock under thermal-hydro-mechanical (THM) coupling condition," *Engineering Geology*, vol. 302, no. 5, 2022.

[12] P. H. S. W. Kulatilake, B. Malama, and J. Wang, "Physical and particle flow modeling of jointed rock block behavior under uniaxial loading," *International Journal of Rock Mechanics and Mining Sciences*, vol. 38, no. 5, pp. 641–657, 2001.

[13] Y. Chen, J. Xu, S. Peng, and F. C. Z. Jiao, "Experimental study on the acoustic emission and fracture propagation characteristics of sandstone with variable angle joints," *Engineering Geology*, vol. 292, no. 10, p. 106247, 2021.

[14] M. M. He, Y. S. Chen, N. Li, and C. H. Zhu, "Deformation and energy characteristics of sandstone under uniaxial cyclic load," *Journal of coal*, vol. 40, no. 8, pp. 1805–1812, 2015.

[15] X. Li, Z. Zhou, T.-S. Lok, and L. T. Hong, "Innovative testing technique of rock subjected to coupled static and dynamic loads," *International Journal of Rock Mechanics and Mining Sciences*, vol. 45, no. 5, pp. 739–748, 2008.

[16] D. Y. Li, C. W. Hu, and Q. Q. Zhu, "Experimental study on dynamic and static combined loading mechanical characteristics and failure law of prefabricated fractured granite," *Journal of rock mechanics and engineering*, vol. 39, no. 6, pp. 1081–1093, 2020.

[17] J. G. Wang, S. F. Liang, and Q. C. Gao, "Experimental study on the influence of joint inclination on impact energy transfer of rock like materials," *Journal of Central South University*, vol. 49, no. 5, pp. 1237–1243, 2018.

[18] R. H. Wang, W. W. Li, and J. Liu, "Influence of joint dip angle on strength and physical characteristics of sandstone," *Journal of Changjiang Academy of Sciences*, vol. 35, no. 6, pp. 70–74+8, 2018.

[19] Q. Ma, Q. Su, and P. Yuan, "Dynamic behavior and energy evolution characteristic of deep roadway sandstone containing weakly filled joint at various angles," *Advances in Civil Engineering*, vol. 2020, no. 6, pp. 1–12, Article ID 8817107, 2020.

[20] H. F. Deng, D. pan, and X. L. Xu, "Study on mechanical properties of intermittent jointed sandstone under triaxial compression," *Journal of geotechnical engineering*, vol. 41, no. 11, pp. 2133–2141, 2019.

[21] B. Pan, X. G. Wang, and Z. Y. Xu, "Study on the influence of joint angle on the dynamic response of rock materials," *Journal of rock mechanics and engineering*, vol. 40, no. 3, pp. 566–575, 2021.

[22] Q. Ping, X. Luo, and Q. Y Ma, "Characteristics of crushing energy consumption of sandstone specimens under impact load," *Journal of rock mechanics and engineering*, vol. 34, no. S2, pp. 4197–4203, 2015.

[23] X. B Li, Z. L Zhou, and Z. Y Ye, "Study on mechanical characteristics of rock under dynamic and static combined loading," *Journal of rock mechanics and engineering*, vol. 27, no. 7, pp. 1387–1395, 2008.

[24] Y. J. Hu, X. Y. Wang, and Z. Zhong, "Experimental study on shear strength characteristics of rough rock joints under variable saturation," *Journal of rock mechanics and engineering*, vol. 41, no. 2, pp. 336–345, 2022.

[25] H. M Zhang, M. Chen, and X. R Qin, "Constitutive model of rock mass considering initial joint damage," *Mining Research and Development*, vol. 41, no. 10, pp. 73–78, 2021.

[26] X. L. Li, J. G. Wang, and Z. Y. Zhang, "Effects of strain rate and joint inclination on dynamic characteristics of rock simulation materials," *Explosion and shock*, vol. 36, no. 4, pp. 483–490, 2016.

[27] S. C Li, L. Wang, and S. C Li, "Experimental study on post peak deformation and failure of rock specimens with different dip angles through joints," *Journal of rock mechanics and engineering*, vol. 32, no. S2, pp. 3391–3395, 2013.

[28] J. Yang, P. Yang, and Y. Yang, "Random vibration and dynamic analysis of a planetary gear train in a wind turbine," *Shock and Vibration*, vol. 2016, no. 12, pp. 1–10, Article ID 6292953, 2016.

[29] Y. Ju, Y. X. Li, and H. P. Xie, "Stress fluctuation and energy dissipation of jointed rock," *Journal of rock mechanics and engineering*, vol. 25, no. 12, pp. 2426–2434, 2006.

[30] "International Society of Rock Mechanics (ISRM)," *Chinese Journal of Rock Mechanics and Engineering*, vol. 1, no. 1, pp. 147-148, 1982.

[31] "Chinese Society for Rock Mechanics and Engineering," 2019, http://www.ttbz.org.cn/Home/S-how/10253.

[32] L. L. Wang, *Foundation of Stress Waves*pp. 39–64, National Defense Industry Press, Beijing, 2nd ed edition, 2010.

[33] X. B. Li, *Rock Dynamics: Fundamentals and Applications*, pp. 258–287, Science Press, Beijing, 2014.